nature physics

SUPPLEMENTARY INFORMATION

https://doi.org/10.1038/s41567-020-0878-9

In the format provided by the authors and unedited.

Enhanced energy coupling for indirect-drive fast-ignition fusion targets

F. Zhang[1,7], H. B. Cai[2,3,7]✉, W. M. Zhou[1], Z. S. Dai[2], L. Q. Shan[1], H. Xu[4], J. B. Chen[1], F. J. Ge[2], Q. Tang[1], W. S. Zhang[2], L. Wei[1], D. X. Liu[1], J. F. Gu[2], H. B. Du[1], B. Bi[1], S. Z. Wu[5], J. Li[1], F. Lu[1], H. Zhang[5], B. Zhang[1], M. Q. He[2], M. H. Yu[1], Z. H. Yang[1], W. W. Wang[1], H. S. Zhang[2], B. Cui[1], L. Yang[1], J. F. Wu[2], W. Qi[1], L. H. Cao[2], Z. Li[1], H. J. Liu[1], Y. M. Yang[1], G. L. Ren[2], C. Tian[1], Z. Q. Yuan[1], W. D. Zheng[2], L. F. Cao[1], C. T. Zhou[5], S. Y. Zou[2], Y. Q. Gu[1]✉, K. Du[1], Y. K. Ding[2], B. H. Zhang[1], S. P. Zhu[1,2,6]✉, W. Y. Zhang[2,3] and X. T. He[2,3]

[1]Science and Technology on Plasma Physics Laboratory, Laser Fusion Research Center, CAEP, Mianyang, China. [2]Institute of Applied Physics and Computational Mathematics, Beijing, China. [3]HEDPS, Center for Applied Physics and Technology, Peking University, Beijing, China. [4]College of Computing Science, National University of Defense Technology, Changsha, China. [5]Center for Advanced Material Diagnostic Technology, Shenzhen Technology University, Shenzhen, China. [6]Graduate School, China Academy of Engineering Physics, Beijing, China. [7]These authors contributed equally: F. Zhang, H. B. Cai. ✉e-mail: cai_hongbo@iapcm.ac.cn; yqgu@caep.cn; zsp@iapcm.ac.cn

Enhanced energy coupling for indirect-drive fast-ignition fusion targets

F. Zhang,[1] H.B. Cai,[2,3,*] W.M. Zhou,[1] Z.S. Dai,[2] L.Q. Shan,[1] H. Xu,[4] J.B. Chen,[1] F.J. Ge,[2] Q. Tang,[1] W.S. Zhang,[2] L. Wei,[1] D.X. Liu,[1] J.F. Gu,[2] H.B. Du,[1] B. Bi,[1] S.Z. Wu,[5] J. Li,[1] F. Lu,[1] H. Zhang,[5] B. Zhang,[1] M.Q. He,[2] M.H. Yu,[1] Z.H. Yang,[1] W.W. Wang,[1] H.S. Zhang,[2] B. Cui,[1] L. Yang,[1] J.F. Wu,[2] W. Qi,[1] L.H. Cao,[2] Z. Li,[1] H.J. Liu,[1] Y.M. Yang,[1] G.L. Ren,[2] C. Tian,[1] Z.Q. Yuan,[1] W.D. Zheng,[2] L.F. Cao,[1] C.T. Zhou,[5] S.Y. Zou,[2] Y.Q. Gu,[1,†] K. Du,[1] Y.K. Ding,[2] B.H. Zhang,[1] S.P. Zhu,[2,1,6,‡] W.Y. Zhang,[2,3] and X.T. He[2,3]

[1]*Science and Technology on Plasma Physics Laboratory, Laser Fusion Research Center, CAEP, 621900, China*

[2]*Institute of Applied Physics and Computational Mathematics, Beijing, 100094, China*

[3]*HEDPS, Center for Applied Physics and Technology, Peking University, Beijing, 100871, China*

[4]*Department of Physics, National University of Defense Technology, Changsha, 410073, China*

[5]*Center for Advanced Material Diagnostic Technology, Shenzhen Technology University, Shenzhen 518118, China*

[6]*Graduate School, China Academy of Engineering Physics, P.O.Box 2101, Beijing 100088, China*

(Dated: March 6, 2020)

SUPPLEMENTARY NOTE 1:

Self-emission radiographic images

Several interesting features in the radiographic images were observed when comparing the self-emission X-ray in the cases with and without short pulse laser. Supplementary Figure 1 shows the time-resolved core plasma self-emission X-ray radiographic images from integrated shots. Here, an 8-image Kirkpatrick-Baez microscope coupled with XFC was used to record these self-emission radiographic images from the diagnose window at the middle of cylindrical hohlraum. Supplementary Figure 1(a) shows the self-emission x-ray from the compressed "tube-shape" pellet, whose image is consistent with the backlighter radiograph image shown in Fig.4(a). In comparison, in the case with the short pulse laser injection shown in Supplementary Figure 1(b), some self-emission on either side of the compressed core from the right-hand-side of the tube-shape pellet can be observed (a clover-like bright area), which is clearly different from the case without the short pulse laser injection in Supplementary Figure 1(b). Here, the clover-like profile of the compressed fuel was regarded as the energy deposition of REB flux generated at the inner tip of cone in the compressed core.

SUPPLEMENTARY NOTE 2:

Hydrodynamic simulations of the compressed "tube-shape" pellet

Two-dimensional radiation hydrodynamic LARED-S [1] simulations have been carried out to study the imploding shell, which are found to reasonably reproduce experimental shell shape under implosion conditions of "high-foot" pulse as in the present experiments. LARED-S is a 2D radiation hydrodynamics code, including laser ray tracing, multi-group radiation diffusion and transport, electron and ion thermal conduction, atomic physics, nuclear reaction, alpha particle transport, and the quotidian equation of state, and so on. Although the x-ray radiography of the compressed fuel showed obvious low-mode asymmetries, the main observed features, such as the peaked value of the compressed density, and "tube-shape" density profile of the compressed pellet are well-captured by our LARED-S simulations by setting a drive P_2 asymmetry with $P_2/P_0 = 25\%$, see Supplementary Figure 2(a). In simulations, the peak compressed density of the fuel is up to $40 g/cm^3$ at peak

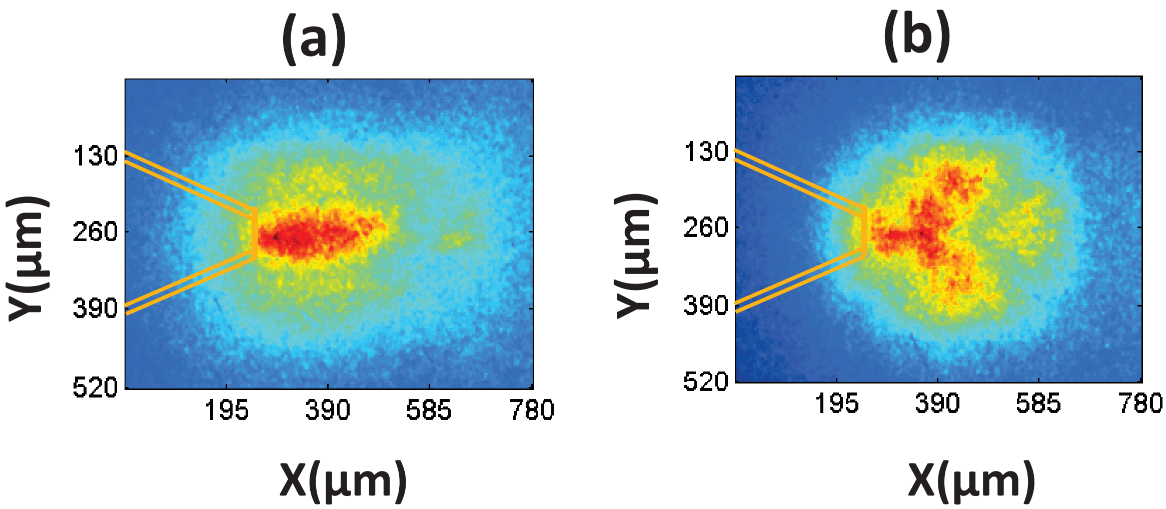

Supplementary Figure 1. Time-resolved core plasma self-emission X-ray radiographic images recorded by Kirkpatrick-Baez microscope. Measured images of core plasma for the cases of (a) without and (b) with short pulse laser injection (shot 16057). The probing time was measured in situ with ±50 ps accuracy. The yellow profile showed position of the gold cone. In the case with short pulse laser (b), a clover-like bright area was presented which was clearly different from case without short pulse laser injection (a).

compression time, which is essentially consistent with the measured data. Note that in Supplementary Figure 2(a), the gold cone is not shown. It is also shown in Supplementary Figure 2(b), the maximum ion temperature can reach as high as 400eV after the compression.

SUPPLEMENTARY NOTE 3:

PIC simulations of the generation of the relativistic electron beam (REB)

To better understand both the characteristics of REB produced by the short pulse laser in the experiments, we have conducted detailed fully relativistic particle-in-cell simulations with the code ASCENT to model, from first principles, the generation of REB. The initial conditions of the preplasma inside the cone targets was imported from the hydrodynamic simulation with XRL2D [2], which is performed to model the actual target geometry and the experimentally measured prepulse, see Supplementary Figure 3(a). Here,

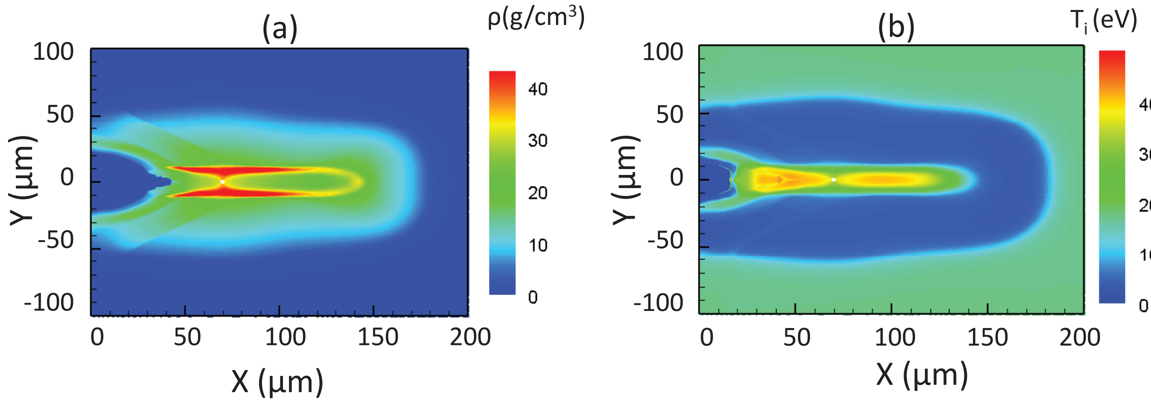

Supplementary Figure 2. Radiation hydrodynamic simulations. Contour plots of simulated (a) fuel mass density (the gold cone is not shown here) and (b) ion temperature at t=5.1ns. These data, together with the parameters of REB simulated by PIC simulations, will be the initial conditions of the hybrid code HEETS.

XRL2D is a two-dimensional non-equilibrium ALE radiation hydrodynamic code, which includes inverse bremsstrahlung absorption and resonant absorption of driving laser, flux-limit heat-conduction approximation and multi-group diffusion approximation, and many micro-processes, such as bremsstrahlung, electron collisional ionization, photo ionization, electron collisional excitation, line emission, dielectronic recombination and their inverse processes. Note that the contrast of the SGIIU short pulse laser, which was measured with a single-shot cross-correlator, was better than 10^8 obtained 80ps before the main pulse [3]. Furthermore, the measured pre-pulse energy was about 20mJ and pulse duration of 2ns. The focus spot of the prepulse is about 20μm (FWHM). The density of the cone wall was clamped at $100n_c$ to avoid the numerical heating. The width of the inner cone wing is $7\lambda_0$ and the width of the gap is $5\lambda_0$. The plasma consists of three species: electrons, protons with $m_p/m_e = 1836$ outside of the cone, and heavy ions (gold ion with an assumed charge state $Z_i = 40$) and $m_{Au}/m_eZ_i = 195.4m_p/40$. The gold cone, whose edge is drawn with the white dashed lines (Supplementary Figure 3(b)), is surrounded by an overdense low-Z plasma. A Gaussian p-polarized laser pulse at $1.5 \times 10^{19} W/cm^2$ intensity and 3ps duration irradiates the target from the left boundary. The intensity profile is Gaussian in the y direction with a spot size of 20μm (FWHM). A typical simulation duration is $1500T_0$, which corresponds to about 5ps for $\lambda_0 = 1.06\mu$m wavelength. The size of the simulation box is $Lx \times Ly = 200\lambda_0 \times 150\lambda_0$

with 10000 × 7500 grid cells.

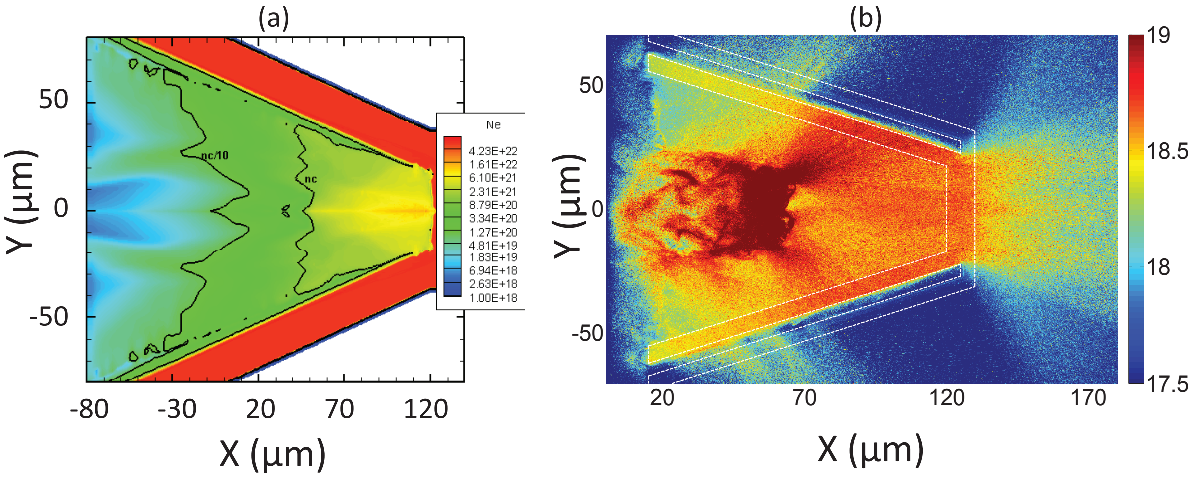

Supplementary Figure 3. Simulations of the preplasma formation inside the cone and the generation of REB. (a) Hydrodynamic code XRL2D simulated pre-plasma density contour plot showing $\sim 80\mu m$ offset distance (see the second solid contour marked with nc) between the critical density and the solid cone tip on axis. (b) PIC code ASCENT simulated forward electron flux in natural logarithm at t=3 ps for the double cone targets with the preplasma read from (a). The gold cone, whose edge is drawn with the white dashed lines, is surrounded by an overdense low-Z plasma initially.

Usually, in the single cone target case, the short pulse laser beam was split into several filaments far from the tip of the cone because of the large preplasma, its propagation was halted and fast electrons were generated with a large angular spread. In contrast, the dynamics of double cone targets lead to a very different picture depending on the formation of the quasistatic magnetic fields inside the vacuum gap [4]; for the double cone target case, most of the fast electrons are collimated and transported to the target rear side, see Supplementary Figure 3(b).

These PIC simulations provided the essential information on the total energy of REB as well as the fraction of energy deposited into REB. PIC simulations showed the total coupling efficiency from laser-to-electron is about 43.1% for p-polarized laser. Here, we took all electrons passing through the "collection board", which locates at $x = 130\mu$m, a place just behind the cone tip. We also selected electrons only with $E > 0.5MeV$ and $v_x > 0$ and $-20 < y[\mu\text{m}] < 20$ in the time domain $t = (0, 5ps)$. It was found that REB has a two-temperature distribution for the energy spectrum $f(E) = A\exp(-E/T_1) + B\exp(-E/T_2)$, with T_1 and T_2 being 0.31 MeV and 1.44 MeV, respectively, and a divergent average polar angle of 47^o. It was estimated that $\eta_e \sim 20.4\%$ of total laser energy converted into this selected REB in the double cone case [4].

It should be pointed out that the reduced dimensionality (2D3V) PIC simulations may overestimate conversion efficiencies compared to 3D PIC simulations [8]. Therefore, we carried out an additional 2D3V PIC simulation with s-polarized laser pulse. And we compared the electron spectra for the cases with the p-polarized and s-polarized laser pulse, which showed the difference of the spectra characteristics between these two cases was small, as shown in Fig. 3(b). For the s-polarized laser case, the conversion efficiency decreases to $\eta_e^s \sim 16.9\%$. The simulated REB temperature was consistent with the measured data shown in Fig. 3(b) (black line for the case without compression).

SUPPLEMENTARY NOTE 4:

Hybrid simulation of the REB transport and deposition

We developed a new, hybrid-PIC code HEETS [5] to model REB transport in the compressed targets, with self-consistent return current and electric and magnetic field generation. HEETS treats the fast electrons by a standard, relativistic PIC method, and describes the background plasma as a reduced two-fluids model. This reduced-model approach is similar to that of Davies [6] and Zuma [7] , The initial plasma conditions (materials, densities, temperatures) for HEETS are transferred from the radiation-hydrodynamic simulations. The REB parameters (energy spectrum, angular spread, flux) are obtained from PIC simulations. The REB parameters are detected at a place just behind the cone tip, see Supplementary Figure 3(b). Supplementary Figure 4(a) shows a schematic map of how we run the hybrid-PIC simulations. Here, the fast electron source was injected at $x = 20\mu$m with parameters given in Supplementary Note 3. The contour plot of ion pressure of the compressed core after heating by REB with an initial state (shown in Supplementary Figure 2) is shown in Supplementary Figure 4(b). Taking advantage of the electrical resistivity gradients caused by the density and temperature inhomogeneities arising during the "tube-shape" fuel compression, our hybrid simulation showed that the quasistatic magnetic fields of the order of

400 $Tesla$ can be generated and serve to collimate REB towards the compressed core. The contour plots of the quasistatic magnetic fields and ion temperature after the injection of REB are shown in Fig. 4(c) and (d) in the paper. As a result, the hybrid simulations showed the deposition efficiency can be significant higher.

Supplementary Figure 4(b) also indicates the energy deposition inside the compressed fuel. In order to show the deposition physics more clearly, we define three different spark regions, as shown in Supplementary Figure 4(b). (1) Region I, as marked by the dark dash-dotted box [$x = (20, 130)\mu$m, and $y = (-15, 15)\mu$m], shows the central high-density compressed fuel region where REB deposited inside. At the positions $y = \pm 15\mu m$, the average density decreases to about half of that in center of the compressed fuel. Moreover, this is also an optimal focal spot radius estimated by $r_b = 60/[\rho/(100\text{g/cm}^3)]^{0.97}\mu$m [9], it gives $r_b \sim 15\mu$m for the case with $\rho \sim 400\text{g/cm}^3$. (2) Region II is marked by the red dashed box [$x = (20, 130)\mu$m, and $y = (-25, 25)\mu$m]. This is also an optimal focal spot radius $r_b \sim 25\mu$m for the case with $\rho \sim 250\text{g/cm}^3$. (3) Region III refers the whole simulation box with $x = (0, 200)\mu$m, and $y = (-100, 100)\mu$m.

Table A I. Comparison of neutron yield in past integrated FI experiments.

E_L(Short pulse)	Y_0	Y_1	T_0 (keV)	ΔT (keV)	Reference
60J	$(9 \pm 1) \times 10^3$	$(2 \pm 1) \times 10^5$	0.4	0.12	Kodama, R. [10]
300J	$(2 \sim 5) \times 10^4$	2×10^7	0.4	0.8	Kodama, R. [11]
300J	$10^4 \sim 10^6$	3.52×10^7	0.67	0.84	Shiraga, H. [12]
613J	$10^5 \sim 10^6$	6.4×10^7	0.8	1.8	Kitagawa, Y. [13]
1000J	3.5×10^6	1.4×10^7	0.12	0.49	Theobald, W. [14]
150J	$(5 \sim 6) \times 10^3$	$(1.7 \pm 0.5) \times 10^6$	0.4	1.4	Our SG-IIU data

In Region I, the deposition efficiency is evaluated as $\eta_D \sim 31.3\%$ and therefore the energy coupling efficiency from laser to the central spark region of the compressed fuel is $\eta = \eta_e * \eta_D \sim 6.4\%$. In Region II, the deposition efficiency is about $\eta_D \sim 46.0\%$ and therefore $\eta = \eta_e * \eta_D \sim 9.4\%$. In Region III, the deposition efficiency is about $\eta_D \sim 67.1\%$ and therefore $\eta = \eta_e * \eta_D \sim 13.6\%$. It is interesting to note that the energy of the escaped

REB in the case with "high-foot" compression is only 34.5% of that in the case without compression in our experiments, which has been shown in Fig. 3(b) in our paper. This means that the deposition efficiency of this REB inside the compressed fuel can be estimated as $1 - 34.5\% = 65.5\%$ from our experiments, which is very close to that evaluated from the hybrid simulations ($\sim 67.1\%$).

Furthermore, the fusion reaction is included in the hybrid simulation, and the neutron yield evaluated by HEETS is 1.6×10^6. This is a reasonable yield which is consistent with the measured neutron yields. Here, in order to make a comparison, we list the previous integrated FI experiments [10–14] in Table A1. One can see that the neutron yields in those experiments are in the order of $10^5 \sim 10^7$. Note that the energy of short pulse laser in these previous experiments is 300J, 300J, 613J, 1000J, respectively. In our SG-IIU experiment, the energy of the short pulse laser is only 150J. As we known, the enhancement of the neutron yield is due to the ion temperature increase resulting from short pulse heating. Therefore, the measured neutron yield of $(1.7 \pm 0.5) \times 10^6$ in our experiment is reasonable. In addition, our hybrid simulation also indicated that a higher neutron yield could be achievable on SG-IIU laser facility by increasing the energy of the short pulse laser, i.e. a neutron yield of 3.2×10^8 could be obtained by increasing the short pulse laser energy to 750J under the same compressed fuel conditions.

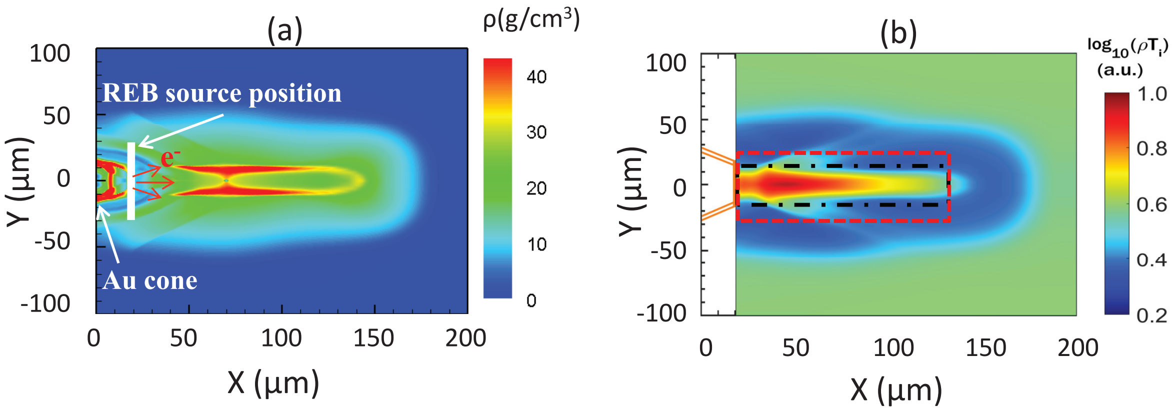

Supplementary Figure 4. Hybrid simulation of the REB transport and deposition. (a) Initial target density in g/cm^3 for hybrid PIC simulations, which are read from hydrodynamic simulations showed in Supplementary Figure 3(a), and (b) the contour plots of ion pressure of the compressed fuel after the injection of REB. The white line in (a) indicates the source cylinder where REB is injected. The dark dash-dotted box (Region I) and red dashed box (Region II) on (b) marked the selected regions for evaluating electron deposition efficiency in hybrid simulations

.

---

* Electronic address: `cai_hongbo@iapcm.ac.cn`

† Electronic address: `yqgu@caep.cn`

‡ Electronic address: `zsp@iapcm.ac.cn`

[1] Pei, W. B. The Construction of Simulation Algorithms for Laser Fusion. Commun. Comput. Phys. **2**, 255 (2007)

[2] Zheng, W.D, and Zhang, G.P, 2D hydrodynamic simulation of a line-focused plasma in Ni-like Ag x-ray laser research. Chin. Phys. **16**, 2439 (2007).

[3] Zhu, J. Q. *et al.* Status and development of high-power laser facilities at the NLHPLP, High Power Laser Sci. Eng. **6**, e55 (2018).

[4] Cai, H. B. *et al.* Enhancing the Number of High-Energy Electrons Deposited to a Compressed Pellet via Double Cones in Fast Ignition, Phys. Rev. Lett. **102**, 245001 (2009).

[5] Xu, H. *et al.*, Control of Fast Electron Propagation in Foam Target by High-Z doping. Plasma

Phys. Control. Fusion **61**, 025010 (2019).

[6] Davies J.R. *et al.*, Laser absorption by overdense plasmas in the relativistic regime. Plasma. Phys. Control. Fusion **51**, 014006 (2009).

[7] Strozzi, D. J. *et al.* Fast-ignition transport studies: Realistic electron source, integrated particle-in-cell and hydrodynamic modeling, imposed magnetic fields, Phys. Plasmas **19**, 072711(2012).

[8] Stark, D.J. *et al.* Effects of dimensionality on kinetic simulations of laser-ion acceleration in the transparency regime. Physics of Plasmas **24**, 053103 (2017).

[9] Atzeni, S. *et al.* A first analysis of fast ignition of precompressed ICF fuel by laser-accelerated protons. Nuclear Fusion **42**, L1 (2002).

[10] Kodama, R. *et al.* Fast heating of ultrahigh-density plasma as a step towards laser fusion ignition. Nature **412**, 798-802 (2001).

[11] Kodama, R. *et al.* Nuclear fusion: Fast heating scalable to laser fusion ignition. Nature **418**, 933-934 (2002).

[12] Shiraga, H. *et al.* Integrated experiments of fast ignition targets by GEKKO-XII and LFEX lasers. High Energy Density Phys **8**, 227-230 (2012).

[13] Kitagawa, Y. *et al.* Direct heating of a laser-imploded core by ultraintense laser-driven ions. Phys. Rev. Lett. **114**, 195002 (2015).

[14] Theobald, W. *et al.* Initial cone-in-shell fast-ignition experiments on OMEGA. Phys. Plasmas **18**, 056305 (2011).